Multiphase Modeling of Bottom-Stirred Ladle for Prediction of Slag–Steel Interface and Estimation of Desulfurization Behavior

UMESH SINGH, RAVIKIRAN ANAPAGADDI, SAURABH MANGAL, KUPPUSWAMY ANANTHA PADMANABHAN, and AMARENDRA KUMAR SINGH

Ladle furnace is a key unit in which various phenomena such as deoxidation, desulfurization, inclusion removal, and homogenization of alloy composition and temperature take place. Therefore, the processes present in the ladle play an important role in determining the quality of steel. Prediction of flow behavior of the phases present in the ladle furnace is needed to understand the phenomena that take place there and accordingly control the process parameters. In this study, first a mathematical model is developed to analyze the transient three-phase flow present. Argon gas bottom-stirred ladle with off-centered plugs has been used in this study. Volume of fluid method is used in a computational fluid dynamics (CFD) model to capture the behavior of slag, steel, and argon interfaces. The results are validated with data from literature. Eye opening and slag–steel interfacial area are calculated for different operating conditions and are compared with experimental and simulated results cited in literature. Desulfurization rate is then predicted using chemical kinetic equations, interfacial area, calculated from CFD model, and thermodynamic data, obtained from the Thermo-Calc software. Using the model, it is demonstrated that the double plug purging is more suitable than the single plug purging for the same level of total flow. The advantage is more distinct at higher flow rates as it leads higher interfacial area, needed for desulfurization and smaller eye openings (lower oxygen/nitrogen pickup).

DOI: 10.1007/s11663-016-0620-2

I. INTRODUCTION

INCREASING emphasis is being placed on producing clean steel in recent years. Ladle secondary steel refining is an important process for ensuring the quality of steel. Inert gas injection is an effective method for homogenizing chemistry, enhancing chemical reaction rates, eliminating thermal stratification, and removing non-metallic inclusions.[1] Argon gas injection from bottom plugs creates the re-circulatory flow that increases mixing of steel and leads to homogenization of chemical constituents and temperature. The argon flow also helps in agglomeration of inclusions and enhances the formation of bigger inclusion particles.[1] These particles then float toward the slag layer at the top of the ladle and stick with it, thereby reducing the inclusion level. Further, rising gas bubbles due to argon flow may cause other phenomena such as breaking of slag layer and formation of eye opening at the top. Due to turbulence, slag layer distorts and enhances intermixing of slag and steel and thereby increasing the interfacial reactions. Most important of these reactions are desulfurization at the interface and oxidation of the melt at the eye opening.

The aim of the present work is to study the flow dynamics in a ladle refining cycle and know its effect on different phenomena such as slag–metal interfacial behavior, eye opening, and emulsification of slag. Further aim is to utilize the calculated interfacial properties from simulations to estimate the kinetics of a few chemical reactions, notable among which is desulfurization. The above phenomena are significantly correlated to the argon flow rate. However, requirements of argon flow are different for different refining operations. Mixing behavior, which is enhanced by the increase in the argon flow, controls the homogenization of composition and temperature. Inclusion agglomeration and floatation require relatively calm flow, whereas better desulfurization efficiency is achieved by a high flow rate which promotes high slag–metal interactions and favorable spout eye area required for the addition of desulfurizer. However, higher flow increases the eye open area which leads to an increase in the oxidation of steel as well as nitrogen pickup from the atmosphere. Moreover, higher degree of turbulence in this case creates instability in the slag layer and increases the refractory wear. This leads to slag entrapment in steel

UMESH SINGH, Scientist, and SAURABH MANGAL, Researcher, are with Tata Consultancy Services Ltd, Pune, India. Contact e-mail: u.singh@tcs.com RAVIKIRAN ANAPAGADDI, Researcher, is with Grace Davison Chemical India Pvt. Ltd, Chennai, India. KUPPUSWAMY ANANTHA PADMANABHAN, University Chair Professor, is with the University of Hyderabad, Hyderabad, India. AMARENDRA KUMAR SINGH, Professor, is with the Indian Institute of Technology Kanpur, Kanpur, India.

Manuscript submitted September 15, 2015.
Article published online February 25, 2016.

and enhances the formation of exogenous inclusions, thus making the steel impure. Therefore, the need is to balance the conflicting requirements for different refining operations which increases the need for multiphase modeling studies.

Various frameworks have been tried to investigate different phenomena during the purging operation in a ladle. Different simulation methods[2–14] have been used to investigate the flow and mixing phenomena. The cold model study[15–20] related to the mixing phenomenon has been used extensively. Detailed reviews of related simulations and cold model studies are found in literature.[21–23] The numerical simulation work in these studies is mostly concentrated on evaluating gas plume flow in a single-phase steel. This kind of treatment involves quasi single-phase,[2–5] Lagrangian–Eulerian[6–10] two-phase, Eulerian two-phase[11–14] studies. A comprehensive review of these models have been presented by Mazumdar and Evans.[24] These models are useful in understanding the gas plume flow and calculation of volume fractions of argon and steel and have been employed in calculations involving inclusion agglomeration and floatation.[25–28] These two-phase models ignore the slag phase and to account for the slag–metal interfacial interactions, simplified macroscopic models have been used in past. However, since slag–metal interactions are complex, macroscopic models are inadequate in predicting interfacial interactions.[21] As forming grades of advanced high strength steels (AHSS) require a precise control of sulfur, a better understanding of the slag–metal interface through separate consideration of slag phase is needed.[15,29] Therefore, transient volume of fluid (VOF) based three-phase models have been employed to simulate slag, steel, and argon phases present in the ladle.[30–33] Using these models, slag eye opening, flow behavior, and distortion of slag–metal interface are studied. More recently, an attempt at estimating the entrainment of slag in the molten steel has also been made.[34]

Desulfurization of liquid steel in a ladle is usually achieved by relatively high level of argon purging. The argon purging creates good level of slag–metal mixing necessary for the desulfurization reaction to take place. In addition to good level of slag–metal mixing, sufficient level of lime saturation in the slag is also required, which is commonly achieved by addition of lime.[35] Usually, desulfurization calculation involves various chemical reactions to estimate activities of different elements. Recently, a coupled computational fluid dynamics (CFD) and thermodynamic model[36–39] was used to incorporate the changes in activities due to spatial variation in elemental concentration. Although this is the most accurate method available for desulfurization modeling, it requires huge computational resources.

In earlier works, desulfurization estimation is done using empirical correlations.[35,40,41] While estimating desulfurization using these correlations, a flat surface is assumed at the interface, which is a crude assumption since the interface distorts and has a wavy character. The distorted interface has higher area which affects the sulfur removal significantly. Therefore, there is a need to establish a coupling between the desulfurization calculation using empirical correlations and utilization of CFD results and thermodynamic data in a low resource-intensive manner.

In this work, a three-phase CFD model is developed on ANSYS Fluent[42] platform to understand the flow phenomenon in an industrial scale ladle. The interaction parameters such as slag–steel interfacial area and eye opening area are computed from the three-phase simulation results obtained from the CFD model. Further, estimation of desulfurization is carried out using thermodynamic data from Thermo-Calc, interfacial area computed from the CFD model, and related empirical correlations. Results of the proposed model are compared with experimental and simulated results cited in literature and show good correspondence.

II. GOVERNING EQUATIONS AND SOLUTION METHODOLOGY

A few assumptions have been made in the present calculations, which are as follows:

1. The geometry of the ladle is assumed to be perfectly cylindrical.
2. The bath is assumed as isothermal and the temperature is set at 1873 K (1600 °C).
3. The liquid steel, slag, and argon have been considered to behave like incompressible Newtonian fluids. Argon, being gas, is compressible. However, in the context of ladle processing, researchers in past have treated argon both compressible[14,32,43] as well as incompressible.[23,25,30,31,43–45] We have treated argon as incompressible fluid as the flow conditions in the ladle has low Mach number and the compressibility factor for argon is acceptably small for the pressure stratification due to height of the liquid steel.
4. Steel and slag are separate phases and individually assumed to be well homogenized. Both are assumed to be at 1873 K (1600 °C) for thermodynamic calculations.
5. The amount of oxygen generated from the desulfurization reaction is calculated by stoichiometry after evaluating the loss of sulfur and assumed to be well mixed in steel.
6. The amount and type of deoxidized product due to generated oxygen in the steel is evaluated thermodynamically.
7. It is assumed that 80 pct of deoxidized product formed in the steel is removed to slag and the rest 20 pct remains in the steel.[25]

The overall solution methodology is presented in Figure 1. The entire framework consists of two main blocks, namely CFD block and desulfurization block. Flow field and volume fractions are calculated using a three-phase CFD model while sulfur removal calculation is done using the desulfurization block. The slag–metal interfacial area, calculated from the simulation results obtained from the CFD model, is utilized in the desulfurization calculation. Sulfur removal calculation is achieved using desulfurization kinetic equation by utilizing different empirical relations and

thermodynamic data from the Thermo-Calc software. The thermodynamic data are accessed at each time interval of desulfurization calculation based on the updated concentration of the elements present in the steel.

A. *CFD Three-Phase Flow Formulation*

A three-dimensional transient mathematical model for argon gas stirred ladle which accounts for the steel, slag, and argon phases has been developed. A set of Navier–Stokes equations with incorporation of volume of fluid (VOF) function has been solved to investigate the dynamic behavior of the three phases. The following set of transport equations[31,32] are solved.

Conservation of mass (continuity equation):

$$\frac{\partial \rho}{\partial t} + \nabla \cdot (\rho \vec{v}) = 0, \quad [1]$$

where ρ is the density of the mixture, t is time, and $\vec{v}$ is the local velocity.

Conservation of momentum:

$$\frac{\partial}{\partial t}(\rho \vec{v}) + \nabla \cdot (\rho \vec{v}\vec{v}) = -\nabla p + \nabla \cdot \left[\mu_e \left(\nabla \vec{v} + \nabla \vec{v}^T\right)\right] + \rho \vec{g} \quad [2]$$

where p is the local pressure, $\vec{g}$ is the acceleration due to gravity, and μ_e is the effective viscosity. The effective viscosity is calculated as sum of dynamic and turbulent viscosities.

Turbulence: κ-ε model

Standard κ-ε model is used to capture the turbulence phenomenon. Following two transport equations of turbulent kinetic energy and its dissipation rate are solved to calculate the effective viscosity.

$$\frac{\partial(\rho k)}{\partial t} + \frac{\partial(\rho k u_i)}{\partial x_i} = \frac{\partial}{\partial x_i}\left[\left(\mu + \frac{\mu_t}{\sigma_k}\right)\frac{\partial k}{\partial x_i}\right] + G_k - \rho\varepsilon, \quad [3]$$

$$\frac{\partial(\rho \varepsilon)}{\partial t} + \frac{\partial(\rho \varepsilon u_i)}{\partial x_i} = \frac{\partial}{\partial x_i}\left[\left(\mu + \frac{\mu_t}{\sigma_\varepsilon}\right)\frac{\partial \varepsilon}{\partial x_i}\right] + C_{1\varepsilon}\frac{\varepsilon}{k}(G_k + C_{3\varepsilon}G_b) - C_{2\varepsilon}\rho\left(\frac{\varepsilon^2}{k}\right) \quad [4]$$

In Eqs. [3] and [4], k is the turbulent kinetic energy, ε is the turbulent kinetic energy dissipation rate, x_i represents the spatial coordinates for different directions. The G_k and G_b terms represent the generation of turbulent kinetic energy due to mean velocity gradient and the generation of turbulent kinetic energy due to buoyancy, respectively. These terms are calculated through Eqs. [5] and [6], respectively.

$$G_k = -\rho u_i u_j \frac{\partial u_i}{\partial x_i}, \quad [5]$$

$$G_b = -g_i(\mu_t/\rho Pr_t)\frac{\partial \rho}{\partial x_i} \quad [6]$$

$$\mu_t = \rho C_\mu \left(\frac{k^2}{\varepsilon}\right) \quad [7]$$

The turbulent viscosity is calculated by Eq. [7] using the k and ε from Eqs. [3] and [4] respectively. In these equations many constants are used whose values are as follows: $C_{1\varepsilon} = 1.44$, $C_{2\varepsilon} = 1.92$, $C_\mu = 1.44$, $\sigma_k = 1.0$, $C_{3\varepsilon} = 1.0$, and $\sigma_\varepsilon = 1.3$.[31,32] Finally,

Volume of Fluid (VOF) model

$$\frac{\partial \alpha_q}{\partial t} + (\vec{v} \cdot \nabla)\alpha_q = 0, \quad [8]$$

$$\alpha_g + \alpha_l + \alpha_s = 1, \quad [9]$$

$$\rho = \alpha_g \rho_g + \alpha_l \rho_l + \alpha_s \rho_s, \quad [10]$$

where α_q and ρ_q are volume fraction and density of the each phase, respectively, in a cell where q can have

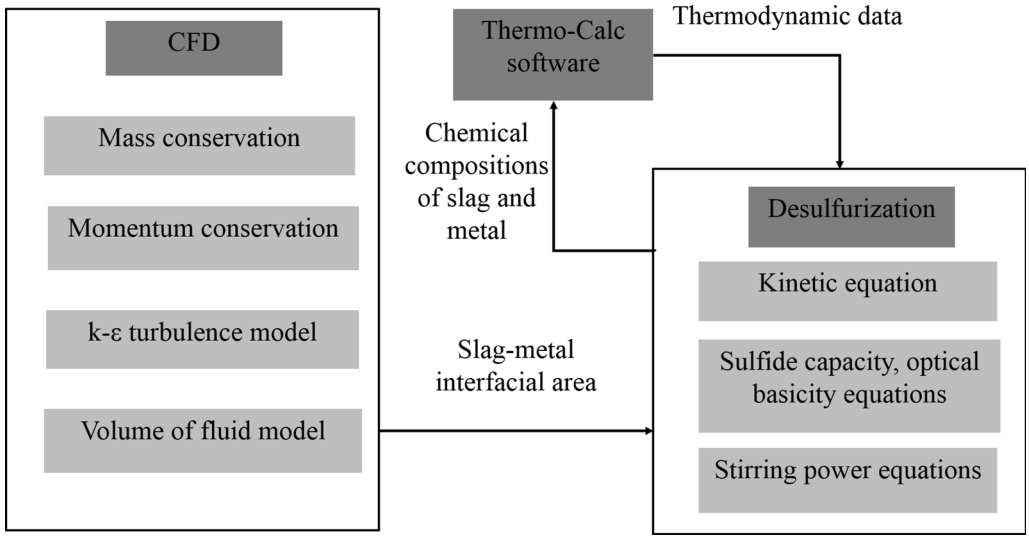

Fig. 1—Solution schematic for CFD and desulfurization calculations.

value of g, l, and s for argon, steel, and slag phases. The VOF formulation assumes that the various phases present in the system are not interpenetrating. Therefore, each phase in a cell is represented by its volume fraction. Volume fractions are derived by solving the continuity equation for each phase given in Eqs. [8] and [9]. The density of the mixture is calculated by Eq. [10] and used in continuity, momentum, and turbulence modeling equations.

The argon gas velocity inlet boundary condition is used at the plugs. The default argon gas flow at the plugs is taken as 200 L/min at STP (denoted by NLM) and corresponding velocity at the plug is used as inlet boundary condition. Bottom and sides of the ladle are considered as walls with no-slip boundary condition and the standard wall function is used to model turbulence near wall region. The slag–metal interface is modeled as a free surface to capture the interfacial behavior. At the top surface opening boundary condition is used through which argon gas can escape. Initial pressure and velocity in the computational domain are set as zero. The initial volume fraction of steel is set as 1 for the liquid steel height. Similarly, initial volume fraction of slag is set as 1 for the slag layer. The initial values of turbulent kinetic energy and turbulent energy dissipation rate are calculated using Eq. [11]. In this equation, V_{in} is the velocity at the plug and D_{plug} is the diameter of the plug.

$$\kappa_{in} = 0.04 V_{in}^2, \quad \varepsilon_{in} = 2\kappa^{1.5}/D_{plug} \qquad [11]$$

Convergence criterion is set as 10^{-4} for all of the variables in the simulations to achieve a converged solution for each time step. It could be known from the calculations that the flow reaches near-steady state after 40 seconds. Therefore, the transient simulation is carried out for 50 seconds to get the solution used for calculating the interfacial area and slag eye opening area.

In the present work, the CFD model is solved using the ANSYS Fluent CFD software.[42] The dimensions of the ladle are given in Table I. In Table II, thermo-physical properties of each of the phases at 1873 K (1600 °C) are available. The ladle under consideration for detailed CFD study is a 220-ton ladle that contains 198 ton molten steel. The argon gas is supplied through an off-centered plug at the bottom with 2/3rd eccentricity. The slag thickness for the base case is assumed to be 100 mm corresponding to 15.3 kg/ton of the weight ratio between slag and steel. The usual slag weight found in the literature is between 13 and 16 kg/ton.[32,40] The rest of the ladle after excluding slag and steel melt is considered to be filled with argon gas.

The computational domain considered for modeling is shown in Figure 2. For achieving grid independent results, different meshes have been used with total number of elements ranging from 55,000 to 350,000. The mesh is refined at the slag–metal interfacial portion as well as near the plugs to capture the gradients smoothly. The suitable grid size at the slag–metal interface is evaluated by comparing simulation results of different grid sizes. The maximum grid size below which the refining of the mesh near interface does not affect simulation results is considered suitable for the current study. The mesh of the computational domain having 260,000 elements with a grid size of 0.01 m near the slag–metal interface and of 0.02 m at plug region is found to be suitable. This mesh is used for all the simulation studies.

B. *Desulfurization Formulation*

Desulfurization in the ladle furnace is mainly achieved through absorption of sulfur into calcium aluminate slag. All the related thermodynamic equations, kinetic equations, and parameters used for desulfurization calculations are given in Table III. The reaction governing this process is given by Eq. [12]. The desulfurization kinetics is determined using reference Eqs. [12] to [13][40] and Eqs. [14] to [20],[35,40,41,46–48] needed for the calculation of the desulfurization rate. The desulfurization process is assumed to be controlled by liquid-phase mass transfer, mentioned in Eq. [12], as this chemical reaction is sufficiently fast. The units for all calculations are taken as SI units, except where another unit is specifically mentioned.

In Eq. [13], [S] is sulfur composition in steel at time instant t, k_s is the mass transfer coefficient, A is the interfacial area between steel and slag, V is the volume of the steel, (S) is the sulfur content in the slag, L_S is the sulfur distribution ratio, t is the time. The relation between the sulfur in slag and sulfur in steel is derived from mass balance and is given by Eq. [14]. In this equation, $(S)_L$ is the final sulfur content in slag, $(S)_0$ is the initial sulfur level in slag, $[S]_O$ is the initial sulfur level in steel, M_L is the (weight of slag)/(weight of steel), k_s is the mass transfer coefficient used for the estimation of mass transfer rate is calculated from Eq. [15][35,41] which, in turn, uses the stirring power ε_s calculated from Eq. [16].[35,41] In this equation, Q is the argon gas purging rate (N m^3/min), W_{st} is the steel weight (ton), H is the height of the steel melt in the ladle (m) from the bottom, T is the temperature of molten steel (K), P_o is the pressure at the top of the ladle (atm). L_S is calculated using Eq. [17].[46] In Eq. [17], C_S is the sulfide capacity which is calculated through Eq. [19].[46,47] Equation 19 is valid for low optical basicity and temperature range of 1673 K to 1973 K (1400 °C to 1700 °C). For higher optical basicity, other correlations[47,48] can be used. The temperature for this study is taken as 1873 K (1600 °C) which is well within the applicable range. $k_{[O]}$ is the equilibrium constant for oxygen reaction and it is calculated through Eq. [18].[46,47] Λ is the average optical basicity of the slag and it is calculated by Eq. [20].[46,47] In this equation Λ_i is the optical basicity of a particular oxide. The optical basicity concept has been used in our calculations for sulfide capacity since it is the best available method at present for determining the basicity of the slag as a single value.[46] The optical basicity of the slag is estimated from the optical basicity of individual oxides to calculate a single value that can be used for further calculations. Spectrographic information and electronegativity data of individual oxides are taken into account while calculating the optical basicity of individual oxides.[46] Moreover, it has been established in the literature that optical basicity can be

Table I. Dimensions of Ladle and Process Parameters Used in CFD and Desulfurization Studies

Parameters	Ref. [31]	Ref. [36]	Unit
Height of ladle	3.82	2.2	m
Bottom diameter	3.36	1.4	m
Top diameter	3.36	1.4	m
Molten steel height	3.26	2.1	m
Slag thickness	0.10	0.09	m
Argon purging rate	25 to 1200 (0.00042 to 0.01667)	80	N L/min (m^3/s)
Plug diameter	0.150	0.05	m
Plug eccentricity	2/3rd	—	—

Table II. Thermo-physical Properties of Different Materials at 1873 K (1600 °C) Used in the CFD and Desulfurization Calculations

Properties	Ref. [31]	Ref. [36]	Unit
Density of molten steel	7020	6982	kg/m^3
Density of argon	0.568	0.568	kg/m^3
Density of slag	3500	3700	kg/m^3
Viscosity of steel	0.0055	0.0055	Pa-s
Viscosity of slag	0.06	0.06	Pa-s
Viscosity of argon	0.000085	0.000085	Pa-s
Gravitation acceleration	9.81	9.81	m/s^2
Temperature of molten steel	1873 K (1600 °C)	1873 K (1600 °C)	K (°C)
Surface tension of metal/slag	1.15	1.15	N/m
Surface tension of metal/argon	1.82	1.82	N/m
Surface tension of slag/argon	0.58	0.58	N/m

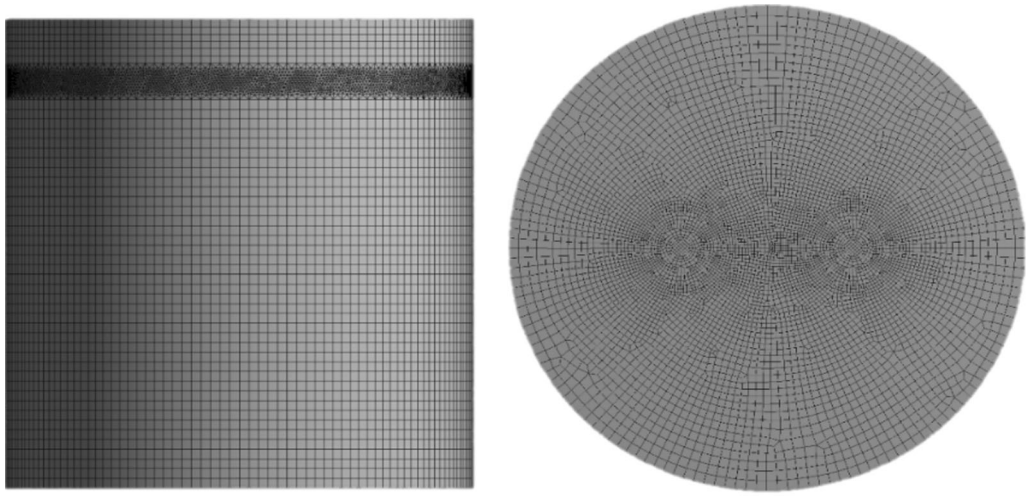

Fig. 2—Geometrical mesh for the ladle (*a*) front view (*b*) top view (the mesh size at the slag–metal interface is 0.01 m and near plug region it is 0.02 m).

well utilized for calculating the sulfide and phosphide capacities.

Steel has certain solubility limit for sulfur. Therefore, the possibility of sulfur removal has to be checked first. The check is done by comparing the actual sulfur content present with the thermodynamic solubility limit. In the next step, desulfurization rate calculation is carried out numerically with the use of Eqs. [12] to [20]. The thermodynamic equilibrium composition of steel and slag will determine the solubility limit at a particular instant. For these calculations, thermodynamic data from the Thermo-Calc software are used.

Table III. Desulfurization: Thermodynamic Equations, Kinetic Equations, and Parameters

Desulfurization reaction[40,41]	$(CaO) + [S] \rightarrow (CaS) + [O]$ (12)
Desulfurization rate[40,41]	$\frac{d[S]}{dt} = -k_s \frac{A}{V}\left([S] - \frac{(S)_L}{L_S}\right)$ (13)
Relation between sulfur in slag to sulfur in steel[36]	$(S)_L = \frac{[S]_O - [S]}{M_L} + (S)_O$ (14)
Mass transfer coefficient (m/s)[35,41]	$k_s = \left\{ \begin{array}{ll} 0.031\varepsilon^{0.25} & \text{if} \quad \varepsilon \leq 60\frac{W}{ton} \\ 8 \times 10^{-6}\varepsilon^{21} & \text{if} \quad \varepsilon > 60\frac{W}{ton} \end{array} \right\}$ (15)
Stirring power (W/ton)[35,41]	$\varepsilon_s = 14.23\left(\frac{QT}{W_{st}}\right)\log\left(1 + \frac{H}{1.48P_o}\right)$ (16)
Sulfur distribution ratio[46]	$L_s = \frac{(C_S k_{[O]})}{[O\,pct]}$ (17)
Equilibrium constant for aluminum oxidation reaction[46,47]	$k_{[O]} = \exp\left(-\frac{935}{T} + 1.375\right)$ (18)
Sulfide capacity equation[46,47]	$\log C_S = \frac{(22{,}690 - 54{,}640\Lambda)}{T} + 43.6\Lambda - 25.2$ (19)
Optical basicity[46,47]	$\Lambda = \sum_{\forall i}\left(\frac{N_{fi} \times (\text{Num. of oxygen atoms in } i)}{\sum_{\forall i} N_{fi} \times (\text{Num. of oxygen atoms in } i)}\right)\Lambda_i$ (20)
Overall desulfurization reaction[35]	$(CaO) + [S] + 2/3[Al] \rightarrow (CaS) + 1/3(Al_2O_3)$ (21)

III. RESULTS AND DISCUSSION

A. *Validation of CFD Model*

Validation of the CFD model is carried out by comparing the results with the simulation results from literature.[31] The ladle processing conditions such as a purging rate of 200 NLM, slag thickness 100 mm, molten steel height 3.26 m have been considered for validation. In Figure 3, the velocity profile in a vertical plane passing through the center of the plug for the single plug ladle is shown. Figure 3(a) represents the literature simulation results,[31] while Figure 3(b) displays the simulation results of this work. From the figure it can be seen that the velocity profile matches well with what is found in literature.

In Table IV, spout height and slag eye opening are compared with the reported results. In the table, eye opening is represented as estimated diameter. It can be seen that the spout heights and eye opening are well matched for both single as well as double plug ladle scenarios. In Table V, eye opening areas obtained from the simulations are compared with simulations from literature[31] as well as macroscopic model[21] results presented for a single plug ladle. Numbers inside the parenthesis represent the approximate diameter of the slag eye opening estimated by assuming that area to be a perfect circle. It can be seen that the eye opening area obtained from the simulations matches well with that found in literature simulations. However, there is a slight variation from the macroscopic models. This is due to the fact that the macroscopic models have limitations when applied to high temperature steel as they are developed using room temperature aqueous flow analysis.[21] These comparisons demonstrate that the CFD model is well validated.

B. *Variations in Eye Opening Area with Design and Process Parameters*

Eye opening plays an important role in determining the cleanliness of the steel. Higher eye opening exposes a higher proportion of liquid metal to the atmosphere. This leads to an increase in the oxidation of steel as well as nitrogen pickup from the atmosphere. Moreover, higher eye opening area increases the slag volume participating in emulsification as more amount of slag mixes with the steel due to downward flow near the eye, as shown in Figure 3(b). This causes slag entrainment in the steel which increases inclusions due to slag breakage. Thus a minimal eye opening is desired during purging operation. Eye opening area increases with an increase in the argon purging rate. This has been illustrated through Figures 4 and 5. The calculated eye opening area is an area with the slag volume fraction less than 10 pct in a horizontal plane at the top of the initial slag layer. The graph in Figure 4 depicts the behavior of eye opening area with respect to argon purging rates for a single plug ladle having 100 mm of slag thickness. From the figure, it is seen that the eye opening area initially increases rapidly for an increase in the purging rate from 25 NLM to 300 NLM. After this level, the rate of increase becomes slow and eye opening area remains nearly unchanged. However, the slag layer breakage starts at higher flow rates which lead to slag entrapment in the steel as shown in Figure 6. Figure 5 reveals that the eye opening area for all the considered cases is lower for the single plug scenarios compared to double plugs scenarios. Further, when eye opening area for an individual eye is compared, eye opening area in case of double plug is substantially smaller. For example, the individual eye opening area in case of double plug is

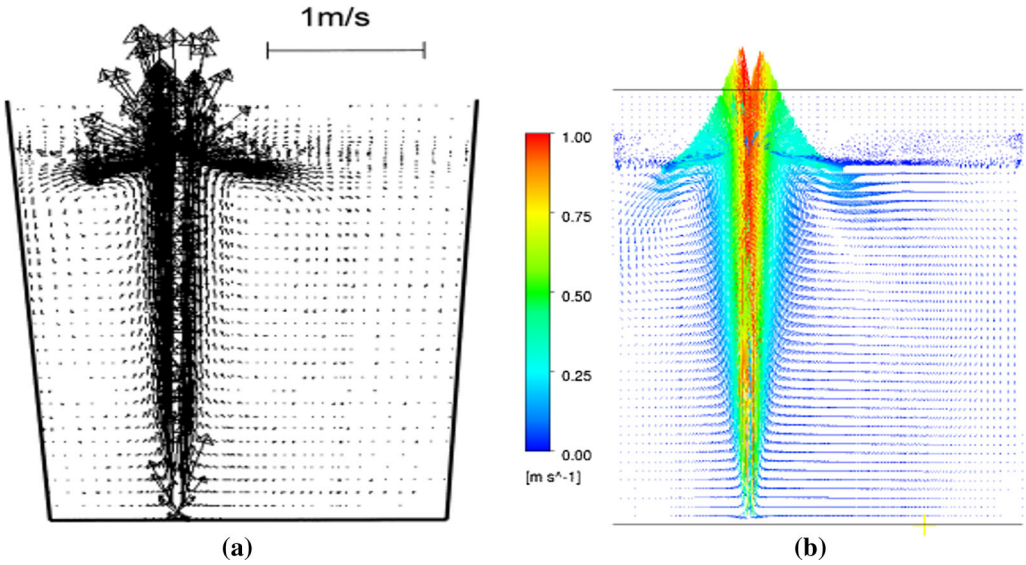

Fig. 3—Comparison of velocity vector with the literature simulation results[31] on a vertical plane passing through the center of the plug for a single plug scenario.

Table IV. Comparison of Spout Height and Eye Opening for Argon Purging Rate of 300 NLM

		Single Plug	Double Plug
Spout height (m)	Present study	0.175	0.170
	Ref. [31]	0.190	0.165
Eye opening diameter (m)	Present study	0.790	0.660
	Ref. [31]	0.810	0.580

Table V. Comparison of Eye Opening Area with Literature Results for Different Argon Purging Rates in a Single Plug Ladle

	Empirical Relation[21]		Present Study Simulations		Literature Simulations[31]
Argon Flow Rate (NLM)	Calculated Area (m^2)	Estimated Diameter (m)	Calculated Area (m^2)	Estimated Diameter (m)	Estimated Diameter (m)
100	0.278	(0.60)	0.160	(0.45)	(0.43)
200	0.401	(0.72)	0.324	(0.64)	(0.66)
300	0.487	(0.79)	0.488	(0.79)	(0.81)

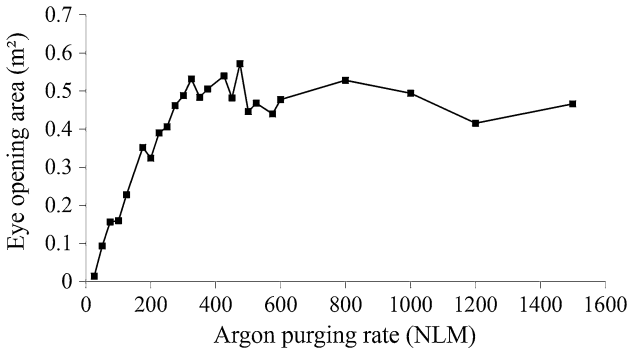

Fig. 4—Comparison of slag eye opening area with respect to argon purging rates for single plug ladle having 100 mm slag thickness.

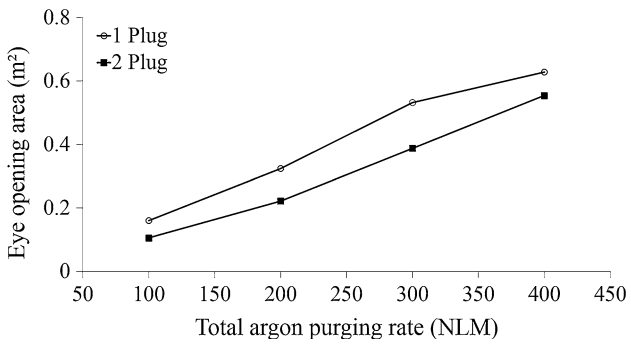

Fig. 5—Comparison of slag eye opening area with respect to argon purging rates for single and double plug ladle having 100 mm slag thickness.

almost one-third of the single plug scenario for the total flow rate of 100 NLM. Moreover, if the comparison of eye opening area for the same individual plug flow rate is made, then also eye opening area in case of 100 NLM individual plug flow is less by almost 30 pct for the case of double plugs (total flow 200 NLM, individual plug flow of 100 + 100 NLM). A similar situation is present for 200 NLM individual plug flow. Moreover, at a higher flow rates, slag breakage (shown in Figure 6) problem starts to happen. Since the double plug with same total flow compared to a single plug has a lower total eye opening and the flow is divided into two plugs, the slag breakage problem can be circumvented as the flow rate is reduced. This suggests that for a higher flow rate, multiple plugs should be used in place of single plug.

In Figure 7, slag volume fraction contours for the case of 100 mm slag thickness are shown in a horizontal plane at a height of 3.36 m from the bottom. In this figure, eye opening is represented with blue color where the volume fraction of slag is very low. The eye area is calculated by estimating the area at the same horizontal plane mentioned above for which slag volume fraction is less than 10 pct. The numbers in the figure are the eye opening area in terms of average diameter. In this figure, also it can be seen that the eye opening area increases with an increase in the purging rate. In addition to that, eye area for a single plug with the same flow rate is higher compared with the same flow in a two plug scenario. Since, a high desulfurization rate requires higher stirring, usually greater than 500 NLM, which may lead to higher amount of slag entrainment due to breakage of slag layer and hamper the cleanliness of the steel. Therefore, from the comparison of results of both Figures 5 and 7 between single and two plugs, one arrives at a conclusion that whenever a higher stirring is required such as for higher level of desulfurization, then multiple plugs are better suited as they can lead to more deformation of slag layer, without leading to breakage of layer, thereby reducing the slag entrainment, while at the same time increasing the interfacial area (explained in Section III–C) for interfacial reactions.

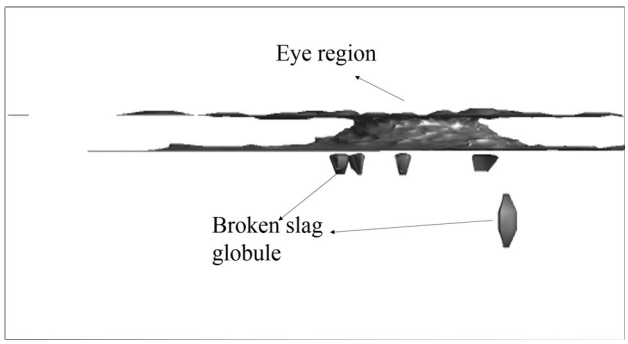

Fig. 6—Iso-surface for 5 pct slag volume fraction for 1000 NLM purging rate to showcase the breakage of slag layer.

The eye opening area is also very much dependent on slag layer thickness. The eye opening behavior for a change in slag layer thickness is shown in Figure 8. It is seen from the figure that at low slag layer thickness, most of the slag is displaced from the top surface, thus eye opening area is more. Further increase in the slag layer thickness decreases the eye opening area but with a slow decrease rate. Similar results can be obtained using an empirical equation[21] where an inverse relation between the eye opening area and slag thickness is obtained, keeping the other parameters constant. However, this empirical equation is applicable only within a narrow limit between the higher and the lowest values of the two variables used to obtain the equation and beyond this range the equation becomes inapplicable. The present method has no such limitations.

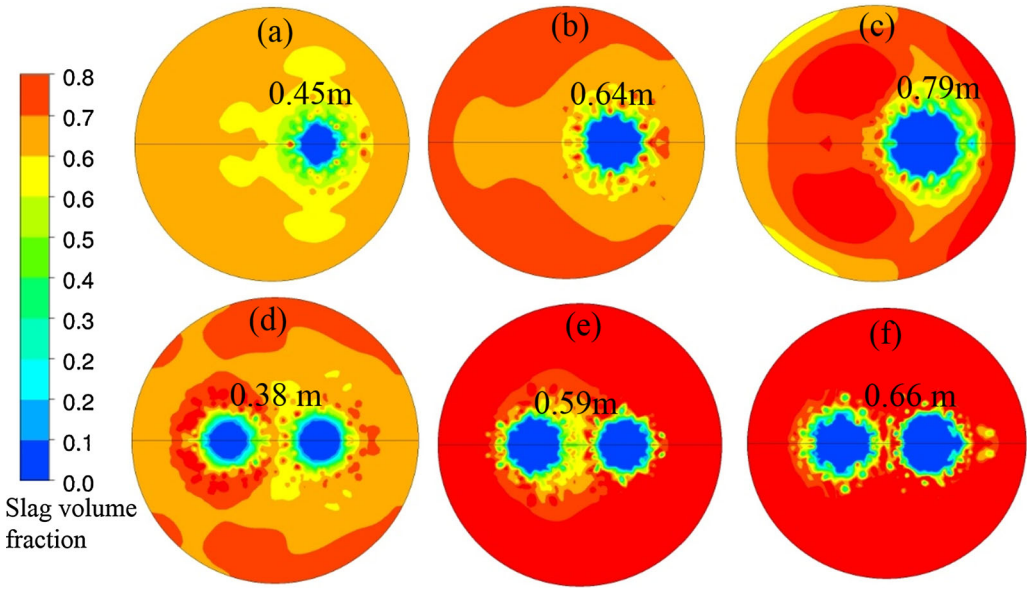

Fig. 7—Slag eye opening diameter in meter (less than 10 pct slag volume fraction) of the individual eye for different purging rates (*a*) 100 NLM (*b*) 200 NLM (*c*) 300 NLM for single plugs and (*d*) 100 + 100 NLM (*e*) 200 + 200 NLM (*f*) 300 + 300 NLM for the double plugs and 100 mm slag thickness.

C. *Behavior of Slag–Metal Interface*

Argon purging creates fluctuations in the slag layer. Higher the rate of flow, more will be the slag layer fluctuations. These fluctuations distort the slag layer and hence lead to an increase in the interfacial area. Since desulfurization reaction and other mass transfer mechanisms such as inclusion removal and dephosphorization reaction take place at the interface, a study of the interfacial behavior becomes important. A comparison of slag–metal interfacial area for a single plug ladle having different slag thicknesses is presented in Figure 9. It can be seen that at low slag thickness the interfacial area is very small. This is because at low thickness most of the slag volume from the top surface is displaced. This leads to bigger eye formation. At the other end, further increase in slag thickness after a certain level does not have much effect on the interfacial area due to the stability provided by the greater weight of the slag.

Figure 10 shows the velocity streamlines on the plane passing through the center of the plug for both plug scenarios. Recirculation of fluid is far more at a higher argon flow rate in a single plug, as shown in Figure 10(a). This leads to more slag entrainment and causes a lowering of the quality of steel, which is not desirable. In case of double plugs scenario, the flow provides some stability to the slag layer as it forms multiple small recirculation, as can be seen from Figure 10(b). This causes more emulsification and distorts the interface, with an attendant increase in the interfacial area. Comparison of slag–metal interfacial area for a ladle having different numbers of plugs is presented in Figure 11. Operating conditions for both the cases like melt height is maintained at 3.26 m and the total argon purging rate is varied from 100 NLM to 400 NLM. In the case of two plugs, each plug is provided with the same flow rate therefore individual plug flow is half compared to single plug flow. From the figure, it can be seen that interfacial area for all the considered cases is higher for the two plug scenarios compared to single plug. Further, interfacial area difference between the two increases up to a total flow rate of 300 NLM. Then for the case of 400 NLM, the difference starts to reduce. This is because the eye formation in case of single plug is bigger for the same total flow rate, which, in turn, reduces the interface area between the slag and the metal. Moreover, the difference between the eye opening areas reduces for higher flow rates as slag layer breakage starts and eye opening saturates as seen from Figure 4. Further, re-oxidation that needs to be avoided for cleaner steel will be higher in a single plug scenario due to larger eye opening. Thus, we can conclude that for higher level of desulfurization double plug scenario is preferred to single plug as it leads to higher level of interfacial area at the same time lowering the total eye opening area (as seen in Figure 5) for the same level of total flow.

Figure 12 shows the variation of the mass transfer coefficient and interfacial area with a change in the argon flow rate. It can be seen from the figure that mass transfer coefficient (k_s) increases near about 50 pct with a change in the flow rate from 100 NLM to 500 NLM. Further, it can also be seen from the figure that with the increase in the argon flow rate, interfacial area first decreases. After certain flow rate it starts to increase. This is happening because at lower flow rates eye opening area dominates and increases with an increase in the flow rate which reduces the interfacial area. But at higher flow rates, eye opening area does not vary much as seen from the Figure 4 and disturbance in the slag layer increases substantially which leads to increase in the interfacial area. Change in slag thickness will not affect the mass transfer coefficient significantly, as it is mainly related to stirring power. However, slag thickness has substantial effect on interfacial area especially for low level of slag layer thicknesses as presented in the Figure 9. Further, minor changes in the geometry of the ladle other than plug positions will not affect the mass transfer coefficient much, as the flow conditions and thereby the stirring power hardly change with minor variations of the ladle geometry.

The volumetric mass transfer coefficient (k_sA) is compared for different flow rates in the Figure 13 to showcase the effect of distorted surface on the interfacial reaction rate for the single plug lade having 100 mm slag layer thickness. It is clear from the figure that the volumetric mass transfer coefficient increases with the increase in the purging rate for both flat and distorted surface. However, the increase is more pronounced at higher flow rates in case of distorted surface as the interface is substantially disturbed at higher flow rate

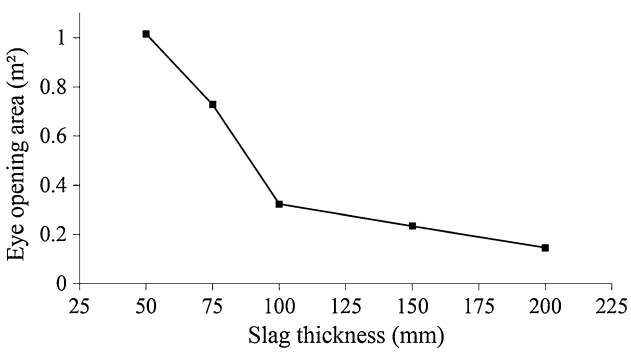

Fig. 8—Comparison of eye opening area for different slag thicknesses for a single plug ladle for 200 NLM argon flow rate.

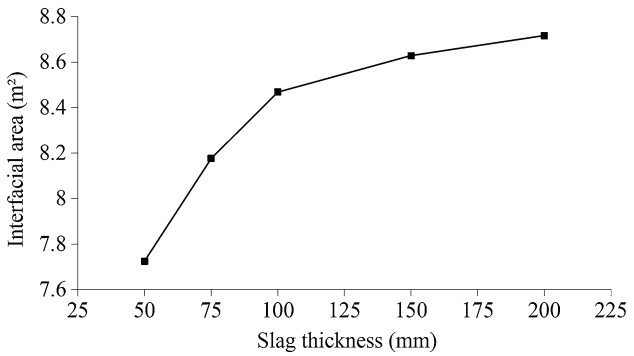

Fig. 9—Slag–metal interfacial area for different slag layer thicknesses for a single plug ladle for 200 NLM argon flow rate.

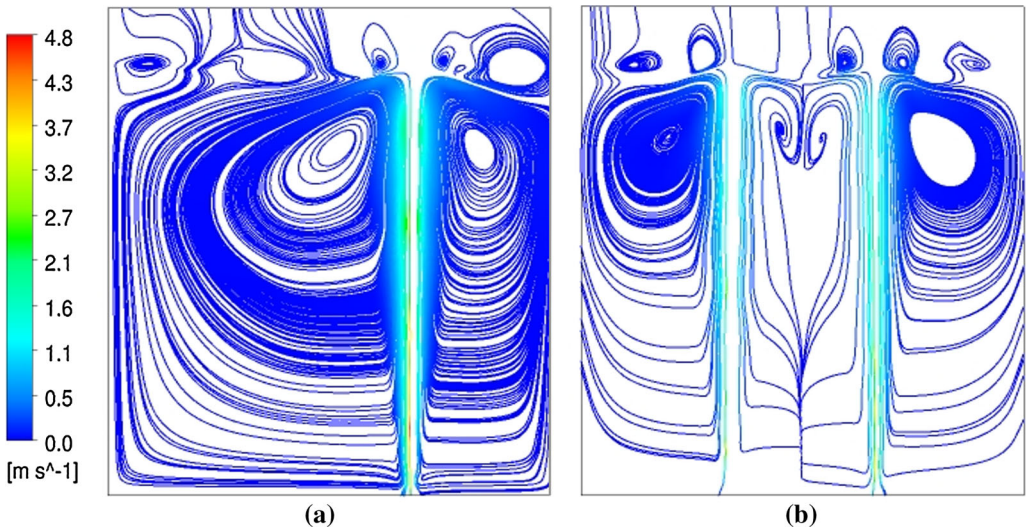

Fig. 10—Comparison of velocity streamlines on a vertical plane passing through the center of the plug (*a*) single plug (*b*) double plug.

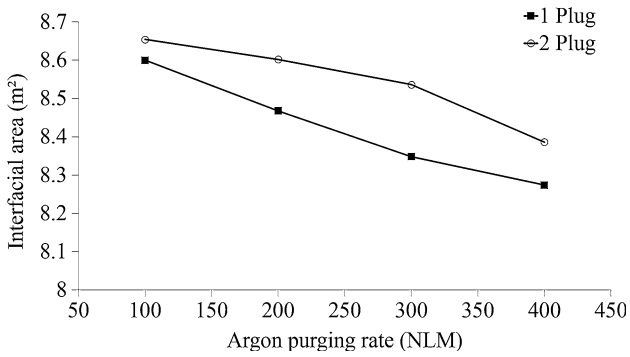

Fig. 11—Slag–metal interfacial area for different argon flow rates for both single and double plugs for 100 mm slag layer thickness.

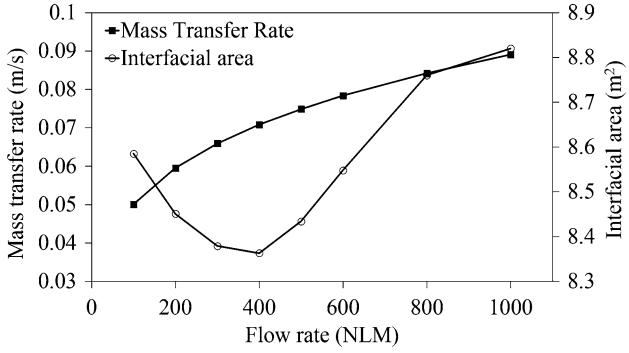

Fig. 12—Comparison of mass transfer coefficient and slag–metal interfacial area with argon flow rates for single plug ladle and slag layer thickness of 100 mm.

that increases the interfacial area. Similar trend has also been reported in the experimental result presented in Reference 22.

D. *Desulfurization Calculations*

Certain grades of steel such as those meant for the manufacture of armor plates, offshore oil pipes, and so on require a low level of sulfur content. A low sulfur level is generally achieved in a ladle refining operation. Desulfurization reaction usually takes place with the involvement of desulfurizers like CaO, which is added in the process. It is present in the slag as it floats up after addition due to its lower density compared with that of steel. Therefore, desulfurization takes place at the slag–metal interface. Very low sulfur concentrations can be achieved by maintaining the slag as saturated in lime. More specifically, slag is maintained as lime saturated calcium aluminate with its SiO_2 concentration not exceeding 10 pct and very low MnO and FeO[35] concentration, *e.g.*, 0.5 pct. The overall desulfurization reaction is represented as Eq. [21].[35] Equations [21] and [12] are one and the same for calculation of desulfurization as liberated oxygen instantly reacts with the

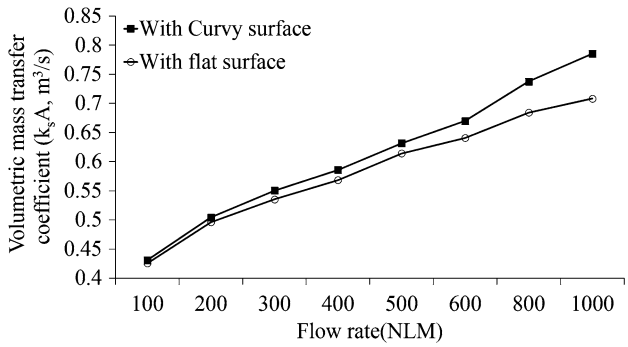

Fig. 13—Comparison of volumetric mass transfer coefficient (k_sA) between the cases having distorted and flat surfaces for the single plug ladle having 100 mm slag layer thickness.

aluminum present in the melt. Therefore, the calculation based on Eq. [12] is taken in the current study, the calculation procedure is presented in Section II–B.

Validation of the desulfurization results is carried out for a separate ladle of dimensions and operating conditions presented in Reference 36. The details of the ladle design and operating conditions from this

reference are summarized in Table I. Thermo-physical properties of different materials at 1873 K (1600 °C) are listed in Table II. The initial chemistry details of the molten steel and slag are given in Tables VI and VII. Other parameters like stirring power, sulfide capacity, and optical basicity used in the desulfurization calculation are also calculated from the equations presented in Table III, again using the abovementioned ladle operating conditions. The interfacial area is taken from the CFD simulation results and thermodynamic data are used from the Thermo-Calc software. For this ladle, the rate of desulfurization obtained is presented in Figure 14. From the figure, it can be seen that desulfurization takes place very fast, and most of the sulfur removal is achieved within 4 to 5 minutes. This suggests that the focus in achieving the desulfurization should be for the initial few minutes only. A comparison of the desulfurization rate with that from literature[36] was made and the trend matches very well, as can be seen from the figure. The plant data for the final sulfur content mentioned in the literature[36] for the same initial composition varied for different heats. It is found to lie between 0.005 to 0.01 pct. The final sulfur content in the current simulation is around 0.0044 pct. Therefore, it is concluded that the present desulfurization formulation predicts the sulfur removal kinetics rather well. There is a slight difference between the current simulation results and the values found by simulations in the literature. It can be attributed to the fact that literature simulations involve coupling of CFD and thermodynamic calculations which captures minor compositional variations near the slag layer. But the coupled CFD and thermodynamic calculations requires higher computational resources. Therefore, current desulfurization formulation is very useful for quick predictions of sulfur content in a limited resource-intensive manner.

In Figure 15, the desulfurization level achieved for different purging rates at the end of 15 minutes of purging operation for the ladle with specifications mentioned in Section II–A is presented. It can be seen from the figure that with an increase in purging rate sulfur removal from steel increases.

The procedure adopted in this study of the desulfurization process has the following new elements. It calculates the interfacial area using a three-phase fluid flow model that captures the variations in the slag–metal interface in a way more accurate than the method of estimating the area by assuming a flat surface. Further, the procedure uses a technique of coupling the thermodynamic data base with empirical relations to include the activity changes due to a change in the bulk concentrations of different elements. For comparison of time required for computation a multicomponent CFD-thermodynamic coupling model is built and simulation time is recorded. During calculations, the same desktop computer is used having four processor and 3GB RAM for comparing the time required for the current methodology and multicomponent CFD-thermodynamic coupling technique. The current method took less than 10 minutes compared with others that took about 3 days. Thus, the present technique is faster while at the same time it gives results not far away from those obtained using the latter time consuming and computationally intensive method. Therefore, it is

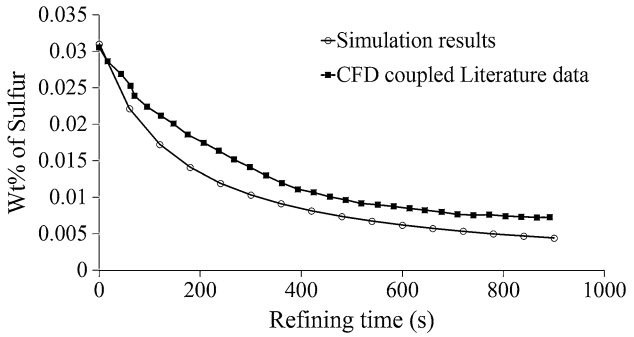

Fig. 14—Comparison of sulfur removal rate with literature[36] simulation data for single plug ladle with 90 mm slag thickness and 80 NLM argon flow.

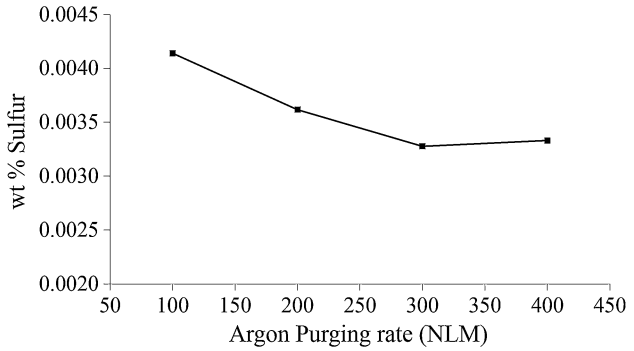

Fig. 15—Comparison of final sulfur content at the end of 15 min of purging operation for different argon flow rates for a single plug ladle and 100 mm slag layer thickness.

Table VI. Initial Steel Chemistry Used in the Desulfurization Calculations[36]

Element	Al	C	Mo	Ni	Cr	Mn	Cu	P	S	O	V
Wt pct	0.052	0.8	0.05	0.14	1.0	0.25	0.16	0.015	0.031	0.00044	0.007

Table VII. Initial Slag Chemistry Used in the Desulfurization Calculations[36]

Element	Al_2O_3	SiO_2	MgO	CaO
Wt pct	30	7.5	7.5	55

possible to use this model for control operations in industrial plants.

IV. SUMMARY

In this work, a three-phase 3-dimensional CFD model is developed for a single as well as two off-center plug scenarios. Fluid flow results obtained from the study have been found to match well with the literature results. The estimates of the slag eye opening area have been validated with both literature as well as macroscopic models and the results are found to match reasonably well. Comparisons of eye opening area and slag–metal interfacial area for different cases of varying slag thicknesses and argon flow rates have been made. The results show that the eye opening area is very much dependent on argon purging rate as well as slag layer thickness. Eye opening area increases with a decrease in the thickness of the slag layer. Similarly, an increase in the argon flow rate also increases the eye opening area. Comparisons of both single and double plug simulation results show that double plug scenario is more suitable for higher flow rates. This is due to the fact that double plug scenario has more surface area as well as lower eye opening area. Double plug cases also lower the chances of slag entrainment due to its creation of multiple smaller recirculation of fluids. Further, Interfacial area is found to be dependent on the slag layer thickness. It is seen that it increases with an increase in the slag layer thickness. However, the rate of increase becomes slower for higher levels of thickness. It is also seen that with the increase in the argon flow rate, interfacial area first decreases and then increases after certain flow rate.

Desulfurization process is formulated by utilizing the actual interfacial area calculated from the three-phase CFD model, instead of simple circular area where a flat interface is assumed. A few empirical equations as well as thermodynamic data generated using the Thermo-Calc software are also made use of. The results obtained from the study show that the sulfur removal activity is fast and most of it is removed within a few minutes. Further, sulfur removal rate increases with an increase in argon purging rate.

NOMENCLATURE

ρ	Density of the mixture (kg/m^3)
ρ_q	Density of each phase q (steel, slag, argon) (kg/m^3)
κ	Local level of turbulent kinetic energy (m^2/s^2)
κ_{in}	Inlet turbulent kinetic energy (m^2/s^2)
ϵ	Local level of turbulent kinetic energy dissipation rate (m^2/s^3)
ϵ_{in}	Inlet turbulent kinetic energy dissipation rate (m^2/s^3)
μ	Dynamic viscosity of molten steel (kg/ms))
μ_t	Turbulent viscosity of molten steel (kg/ms)
μ_e	Effective viscosity of molten steel (kg/ms)
α_q	Volume fraction of particular phase q
Λ	Average optical basicity of the slag
Λ_i	Optical basicity of individual oxides
ϵ_s	Stirring power (W/ton)
A	Interfacial area between slag and steel (m^2)
(CaO)	CaO in the slag
(CaS)	CaS in the slag
C_S	Sulfide capacity of slag
D_{plug}	Diameter of the plug (m)
G_k	Generation of turbulent kinetic energy due to mean velocity gradient
G_b	Generation of turbulent kinetic energy due to buoyancy
g	Acceleration due to gravity (m/s^2)
H	Height of liquid steel melt (m)
k_s	Mass transfer rate (m/s)
$k_{[O]}$	Equilibrium constant of aluminum oxidation reaction
L_S	Sulfur distribution ratio
M_L	Ratio of slag to steel weights
NLM	Argon flow rate in Liter/Minute at STP
N_{fi}	Mole fraction of the particular oxide in the slag
[O]	Dissolved oxygen in the melt
[O pct]	Oxygen concentration in the liquid steel melt (wt pct)
p	Local pressure in the fluid (pa)
P_o	Pressure at the top of the Ladle (atm)
Pr_t	Prandtl number
q	Phase notations l: Liquid steel, g: argon gas, s: slag
Q	Argon flow rate (N m^3/s)
[S]	Sulfur composition in the steel melt (wt pct)
(S)	Sulfur content in the slag (wt pct)
$[S]_L$	Final sulfur content in slag (wt pct)
$[S]_0$	Initial sulfur content in slag(wt pct)
T	Temperature (K)
t	Time instant (s)
u_i	Velocity component of the fluid (m/s)
v	Local velocity (m/s)
V_{in}	Inlet velocity at the plug (m/s)
V	Volume of steel (m^3)
W_{st}	Weight of liquid steel (ton)

REFERENCES

1. J. Aoki, L, Zhang, and B.G. Thomas: *3rd International Congress on Science and Technology of Steel Making*, 2005, pp. 319–32.
2. S. Ganguly and S. Chakraborty: *ISIJ Int.*, 2004, vol. 44 (3), pp. 537–46.
3. S. Ganguly and S. Chakraborty: *Ironmaking Steelmaking*, 2008, vol. 35 (7), pp. 524–30.
4. S. Joo and R.I.L. Guthrie: *Metall. Trans. B*, 1992, vol. 23B, pp. 765–78.
5. M.Y. Zhu, I. Inomoto, N. Yamasaki, and T.C. Hsiao: *ISIJ Int.*, 1996, vol. 36 (5), pp. 503–11.
6. S. Johansen and F. Boysan: *Metall. Mater. Trans. B*, 1988, vol. 19B, pp. 755–64.
7. J. Aoki, B. G. Thomas and J. Peter: AISTech, Assoc. Iron Steel Technology, 2005, Warrendale, PA, pp. 1047-1056.
8. M. Warzecha, J. Jowsa, P. Warzecha, and H. Pfeifer: *Steel Res. Int.*, 2008, vol. 79 (11), pp. 852–60.

9. M. Madan, D. Satish, and D. Mazumdar: *ISIJ Int*., 2005, vol. 45 (5), pp. 677–85.
10. D. Guo, L. Gu, and G. Irons: *Appl. Math. Model*., 2002, vol. 26, pp. 263–80.
11. D. Mazumdar, R. Yadav, and B.B. Mahato: *ISIJ Int*., 2002, vol. 42 (1), pp. 106–08.
12. M.R. Davidson: *Appl. Math. Model*., 1990, vol. 14, pp. 67–76.
13. H. Turkoglu and B. Farouk: *Metall. Trans. B*, 1990, vol. 21B, pp. 771–81.
14. W. Lou and M. Zhu: *Metall. Mater. Trans. B*, 2013, vol. 44B, pp. 1251–63.
15. C.G. Mendez, N. Nigro, and A. Cardona: *J. Mater. Process. Technol*., 2005, vol. 160, pp. 296–305.
16. J. Mandal, S. Patil, M. Madan, and D. Mazumdar: *Metall. Mater. Trans. B*, 2005, vol. 36B, pp. 479–87.
17. S.G.A. Brooks and G.A. Irons: *Iron Steel Inst. Jpn. Int*., 2003, vol. 43, pp. 262–63.
18. D. Mazumdar and J.W. Evans: *Metall. Mater. Trans. B*, 2004, vol. 35B, pp. 400–04.
19. K. Krishnapisharody and G.A. Irons: *Metall. Mater. Trans. B*, 2006, vol. 37B, pp. 763–72.
20. K. Krishnapisharody and G.A. Irons: *ISIJ Int*., 2008, vol. 48, pp. 1807–09.
21. D. Mazumdar and J.W. Evans: *ISIJ Int*., 2004, vol. 44 (3), pp. 447–61.
22. D. Mazumdar and R.I.L. Guthrie: *ISIJ Int*., 1995, vol. 35 (1), pp. 1–20.
23. D. Sichen: *Steel Res. Int*., 2012, vol. 83 (9), pp. 825–41.
24. D. Mazumdar and J.W. Evans: *Modelling of Steel Making Process*, CRC Press Taylor & Francis Group, London, 2004, p. 175.
25. D.Q. Geng, H. Lei, and J.C. He: *ISIJ Int*., 2010, vol. 50 (11), pp. 1597–1605.
26. J. Aoki, L. Zhang, and B.G. Thomas: *3rd International Congress on Science & Technology of Steelmaking, Association for Iron & Steel Technology*, 2005, pp. 319–32.
27. J.P. Bellot, V.D. Felice, B. Dussoubs, A. Jardy, and S. Hans: *Metall. Mater. Trans. B*, 2014, vol. 45B, pp. 13–21.
28. W. Lou and M. Zhu: *Metall. Mater. Trans. B*, 2013, vol. 44B, pp. 762–82.
29. S.W.P. Cloete, J.J. Eksteen, and S.M. Bradshaw: *Prog. Comput. Fluid Dyn. Int. J*., 2009, vol. 9 (6–7), pp. 345–56.
30. C.A. Llanos, S. Garcia-Hernandez, J.A. Ramos-Banderas, J. de Barreto, and G. Solorio-Diaz: *ISIJ Int*., 2010, vol. 50 (3), pp. 396–402.
31. B. Li, H. Yin, C.Q. Zhou, and F. Tsukihashi: *ISIJ Int*., 2008, vol. 48 (12), pp. 1704–11.
32. H. Liu, Z. Qi, and M. Xu: *Steel Res. Int*., 2011, vol. 82 (4), pp. 440–58.
33. S.W.P. Cloete, J.J. Eksteen, and S.M. Bradshaw: *Miner. Eng*., 2013, vols. 46–47, pp. 16–24.
34. A. Huang, H. Harmuth, M. Doletschek, S. Vollmann, and X. Feng: *Steel Res. Int*., 2015, vol. 86 (12), pp. 1147–454.
35. E.T. Turkdogan: *Fundamentals of Steelmaking*, The Institute of materials, London, 1996, p. 245.
36. L. Jonsson, D. Sichen, and P. Jonsson: *ISIJ Int*., 1998, vol. 38 (3), pp. 260–67.
37. M.A.T. Andersson, L.T.I. Jonsson, and P.G. Jonsson: *ISIJ Int*., 2000, vol. 40 (11), pp. 1080–88.
38. W. Lou and M. Zhu: *ISIJ Int*., 2015, vol. 55 (5), pp. 961–69.
39. W. Lou and M. Zhu: *Metall. Mater. Trans. B*, 2014, vol. 45B, pp. 1706–22.
40. A. Ghosh: *Secondary Steelmaking, Principles and Applications*, CRC Press LLC, New York, 2001, p. 200.
41. R.J. Fruehan: *The Making, Shaping and Treating of Steel,* 11th ed., The AISE Steel Foundation, Pittsburgh, 1998, p. 661.
42. ANSYS® Academic Research, Fluent, Release 15.
43. M.B. Goldschmit and G.N. Venturini: *European Congress on Computational Methods in Applied Sciences and Engineering*, Jyvaskyla, 2004.
44. L. Zhang: *JOM*, 2012, vol. 64 (9), pp. 1059–62.
45. Z. Zhang: PhD thesis, 2010, Department of Materials Science and Engineering, Royal Institute of Technology, Stockholm, Sweden.
46. E. Pretorius: *Fundamentals of EAF and Ladle Slags and Ladle Refining Principles, Bakers Refractories.*
47. Z. Slovic, K.T. Raic, L. Nedeljkovic, and T.V. Husovic: *Mater. Technol*., 2012, vol. 46, pp. 683–88.
48. M. Andersson, P.G. Jonsson, and M.M. Nzotta: *ISIJ Int*., 1999, vol. 40 (11), pp. 1140–49.